A&A 418, 1171–1178 (2004)
DOI: 10.1051/0004-6361:20034198

Astronomy & Astrophysics

K-shell photoionization and electron impact excitation of Fe XVII–Fe XXIII⋆

M. A. Bautista[1], C. Mendoza[1], T. R. Kallman[2], and P. Palmeri[2,⋆⋆]

[1] Centro de Física, Instituto Venezolano de Investigaciones Científicas (IVIC), PO Box 21827, Caracas 1020A, Venezuela
[2] NASA Goddard Space Flight Center, Code 662, Greenbelt, MD 20771, USA

Received 14 August 2003 / Accepted 30 October 2003

Abstract. Photoabsorption cross sections across the K edge of Fe XVII–Fe XXIII and electron impact K-shell excitation effective collision strengths in Fe XVIII–Fe XXIII have been computed with the Breit-Pauli R-matrix method. The target models are represented with all the fine-structure levels within the $n = 2$ complex, built up from single-electron orbital bases obtained in a Thomas-Fermi-Dirac statistical model potential. The effects of radiation and spectator Auger dampings are taken into account by means of an optical potential. In photoabsorption, these effects cause the resonances converging to the K thresholds to display symmetric profiles of constant width that smear the edge, with important implications in spectral analysis. In collisional excitation, they attenuate resonances making their contributions to the effective collision strength practically negligible.

Key words. atomic data – atomic processes – line: formation

1. Introduction

Recent improvements in the spectral capabilities and sensitivity of satellite-borne X-ray telescopes (*Chandra*, *XMM-Newton*) have promoted the role of Fe K lines in plasma diagnostics, a trend that will continue to grow with the launch of future instruments such as *Astro-E2* and *Constellation-X*. These diagnostics ultimately rely on the knowledge of the microphysics of line formation and hence on the accuracy of the atomic data. In this respect, Bautista et al. (2003) (hereafter Paper I), Palmeri et al. (2003a) (hereafter Paper II), Palmeri et al. (2003b) and Mendoza et al. (2004) have computed complete data sets of level energies, wavelengths, A-values and Auger rates for K lines in Fe II–Fe XXV. However, realistic spectral modeling also requires data for the population mechanisms, namely photoabsorption, photoionization and electron impact excitation cross sections. The K-resonance behavior in these continuum processes in both lowly and highly ionized species is somewhat different from that displayed by the outer-electron resonance series. For instance, Gorczyca (2000), Gorczyca & McLaughlin (2000) and Palmeri et al. (2002) (hereafter Paper III) have shown that the K-resonance widths are dominated by radiative and Auger dampings that make them independent of the principal quantum number and cause a smearing of the edge. Paper III shows the possibility of devising diagnostics based on K-edge broadening, but these would necessarily rely on accurate high-energy photoabsorption cross sections. Most previous close-coupling calculations of high-energy continuum processes in Fe ions (Berrington et al. 1997; Donnelly et al. 2000; Berrington & Ballance 2001; Ballance et al. 2001) have completely ignored spectator Auger decay, the main contributor of the K-resonance width.

In the present work we have carried out extensive calculations of the photoabsorption and photoionization of Fe XVII–Fe XXIII, considering both the total cross sections and partial cross sections where the daughter ion is left in a photoexcited K-vacancy state. Effective collision strengths for excitation by electron impact have also been computed. Calculations have been carried out with two relativistic numerical approaches: the Breit-Pauli R-matrix (BPRM) method and AUTOSTRUCTURE based on a Thomas-Fermi-Dirac statistical model potential. In all these calculations, damping effects are given special care.

2. Numerical methods

The present relativistic calculations are performed with a Breit-Pauli Hamiltonian which for an N-electron system is given by

$$H_{\rm bp} = H_{\rm nr} + H_{\rm 1b} + H_{\rm 2b} \quad (1)$$

where $H_{\rm nr}$ is the usual non-relativistic Hamiltonian. The one-body relativistic operators

$$H_{\rm 1b} = \sum_{n=1}^{N} f_n({\rm mass}) + f_n({\rm d}) + f_n({\rm so}) \quad (2)$$

Send offprint requests to: M. A. Bautista,
e-mail: bautista@kant.ivic.ve

⋆ Tables 1 to 6 are only available in electronic form at the CDS via anonymous ftp to cdsarc.u-strasbg.fr (130.79.128.5) or via http://cdsweb.u-strasbg.fr/cgi-bin/qcat?J/A+A/418/1171

⋆⋆ Research Associate, Department of Astronomy, University of Maryland, College Park, MD 20742, USA.

represent the spin-orbit interaction, f_n(so), and the non-fine structure mass-variation, f_n(mass), and one-body Darwin, f_n(d), corrections. The two-body corrections

$$H_{2b} = \sum_{n>m} g_{nm}(\mathrm{so}) + g_{nm}(\mathrm{ss}) + g_{nm}(\mathrm{css}) + g_{nm}(\mathrm{d}) + g_{nm}(\mathrm{oo}), \quad (3)$$

usually referred to as the Breit interaction, include, on the one hand, the fine structure terms g_{nm}(so) (spin-other-orbit and mutual spin-orbit) and g_{nm}(ss) (spin-spin); and on the other, the non-fine structure terms g_{nm}(css) (spin-spin contact), g_{nm}(d) (Darwin) and g_{nm}(oo) (orbit-orbit).

2.1. BPRM

The Breit-Pauli R-matrix package (BPRM) is widely used in electron-ion scattering and in radiative bound-bound and bound-free calculations. It is based on the close-coupling approximation of Burke & Seaton (1971) whereby the wavefunctions for states of an N-electron target and a colliding electron with total angular momentum and parity $J\pi$ are expanded in terms of the target eigenfunctions

$$\Psi^{J\pi} = \mathcal{A} \sum_i \chi_i \frac{F_i(r)}{r} + \sum_j c_j \Phi_j. \quad (4)$$

The functions χ_i are vector coupled products of the target eigenfunctions and the angular components of the incident-electron functions; $F_i(r)$ are the radial part of the continuum wavefunctions that describe the motion of the scattered electron and $\mathcal{A}$ is an antisymmetrization operator. The functions Φ_j are bound-type functions of the total system constructed with target orbitals; they are introduced to compensate for orthogonality conditions imposed on the $F_i(r)$ and to improve short-range correlations. The Kohn variational principle gives rise to a set of coupled integro-differential equations that are solved by R-matrix techniques (Burke et al. 1971; Berrington et al. 1974, 1978, 1987) within a box of radius $r \le a$, say. In the asymptotic region ($r > a$), exchange between the outer electron and the target ion is neglected, and the electrostatic potential can be expanded in terms of multipole long-range potentials which are dominated for large values of r by the Coulombic term. If all long-range potentials beyond the Coulombic are neglected, the one-electron wavefunction can be expressed in terms of regular and irregular Coulomb functions. Further computations of the contributions of long-range potentials can be then carried out by perturbation techniques. The reactance K-matrix and the scattering S-matrix, from which cross sections are determined, are generated by matching at the box boundary the inner radial solutions to linear combinations of the outer-region Coulomb functions. The choice of the R-matrix boundary radii is typically made such that the amplitudes of the target orbitals at the boundary have fully decayed. When computing cross sections for inner-shell processes, it is important to include sufficient continuum functions in the truncated expansion (4) to ensure convergence.

Breit-Pauli relativistic corrections have been introduced in the R-matrix suite by Scott & Burke (1980) and Scott & Taylor (1982), but the two-body terms (see Eq. (3)) have not as yet been implemented. Inter-channel coupling is equivalent to configuration interaction (CI) in the atomic structure context, and thus the BPRM method provides a formal and unified approach to study the decay properties of both bound states and resonances.

2.2. AUTOSTRUCTURE

AUTOSTRUCTURE, an extension by Badnell (1986, 1997) of the atomic structure program SUPERSTRUCTURE (Eissner et al. 1974), computes fine-structure level energies, radiative and Auger rates in a Breit-Pauli relativistic framework. Single electron orbitals, $P_{nl}(r)$, are constructed by diagonalizing the non-relativistic Hamiltonian, $H_{\rm nr}$, within a statistical Thomas-Fermi-Dirac model potential $V(\lambda_{nl})$ (Eissner & Nussbaumer 1969). The λ_{nl} scaling parameters are optimized variationally by minimizing a weighted sum of the LS term energies. LS terms are represented by CI wavefunctions of the type

$$\Psi(LS) = \sum_i c_i \phi_i. \quad (5)$$

Continuum wavefunctions are constructed within the distorted-wave approximation. Relativistic fine-structure levels and rates are obtained by diagonalizing the Breit-Pauli Hamiltonian in intermediate coupling. The one- and two-body operators have been fully implemented to order $\alpha^2 Z^4$ where α is the fine-structure constant and Z the atomic number.

3. Radiation and Auger dampings

When a K-vacancy state in an Fe ion with a partially filled L shell is populated by dielectronic recombination or photon excitation

$$\left\{ \begin{array}{l} \mathrm{Fe}^{(\chi+1)+}\ [2]^{p+1} + \mathrm{e}^- \\ \mathrm{Fe}^{\chi+}\ [2]^p + h\nu \end{array} \right\} \rightarrow\ \mathrm{Fe}^{\chi+}\ [1][2]^p\ nl, \quad (6)$$

where $[n]^p$ denotes p vacancies in the n shell, it decays by both autoionization (Auger decay) and fluorescence

$$\begin{aligned} \mathrm{Fe}^{\chi+}\ [1][2]^p\ nl\ &\rightarrow\ \mathrm{Fe}^{(\chi+1)+}\ [2]^{p+1} + \mathrm{e}^- && (7)\\ &\rightarrow\ \mathrm{Fe}^{(\chi+1)+}\ [2]^{p+2}\ nl + \mathrm{e}^- && (8)\\ &\rightarrow\ \mathrm{Fe}^{\chi+}\ [2]^p + h\nu && (9)\\ &\rightarrow\ \mathrm{Fe}^{\chi+}\ [2]^{p+1}\ nl + h\nu. && (10) \end{aligned}$$

The participator KLn Auger channels (Eq. (7)) can be adequately represented in the BPRM method by including in the close-coupling expansion (4) configuration-states of the $\mathrm{Fe}^{(\chi+1)+}$ target with $n \le 2$. On the other hand, in the KLL Auger process in Eq. (8), also referred to as spectator Auger decay, the nl Rydberg electron remains a spectator. Its formal handling within the close-coupling approach is thus severely limited to low-n resonances as it implies the inclusion of target states with nl orbitals. Moreover, it has been recently shown in Paper III that KLL is the dominant Auger decay mode in the Fe sequence by no less than 75%, and leads to photoabsorption cross sections at high energies dominated by damped resonances of constant widths as $n \rightarrow \infty$ which cause the smearing of the

edge. Transitions in Eqs. (9) and (10) lead to radiation damping. The former, referred to as the Kn transition array ($n > 2$), is driven by the np $\rightarrow$ 1s optical electron jump. The latter is the Kα transition array (2p $\rightarrow$ 1s) where again the nl Rydberg electron remains a spectator, its large widths therefore being practically independent of n (Paper II).

The present treatment of Auger and radiative dampings within the BPRM framework uses the optical potential described by Gorczyca & Badnell (1996, 2000) where the resonance energy with respect to the threshold energy acquires an imaginary component. For example, the energy of the $[1][2]^p$ nl closed channel is now expressed as

$$E_1 \rightarrow E_1 - \mathrm{i}(\Gamma_1^a + \Gamma_1^r)/2 \tag{11}$$

with Γ_1^a and Γ_1^r being respectively the Auger and radiative widths of the $[1][2]^p$ core. In the case of radiation damping, the optical potential modifies the R-matrix to the complex form

$$R_{jj'}(E) = R^0_{jj'}(E) + 2\sum_{nn'} d^0_{jn} d^0_{j'n'} (\gamma^{-1})_{nn'} \tag{12}$$

where $R^0_{jj'}$ are the R-matrix elements without damping, d^0_{jn} are $(N+1)$-electron dipole matrix elements and γ^{-1} is a small inverted complex matrix defined in Eq. (100) of Robicheaux et al. (1995).

4. Results

The present BPRM calculations have been carried out with the standard R-matrix computer package of Berrington et al. (1995) for the inner region and with the asymptotic codes STGFDAMP (Gorczyca & Badnell 1996) and STGBF0DAMP (Badnell, unpublished) for determining photoabsorption and electron impact cross sections that take into account the effects of radiation and Auger dampings. This numerical approach has been previously used in Paper I to compute the high-energy photoabsorption cross section of the ground state of Fe XXIII and effective collision strengths for Fe XXIV.

Target representations include all the possible fine structure levels with $n \leq 2$, constructed in AUTOSTRUCTURE with single-electron orbital bases obtained by minimizing the sum of the corresponding LS term energies. Radiative and Auger widths have been taken from Paper II. The calculations for all ions involve 30 continuum orbitals and R-matrix boundary radii that vary from 1.0 au for Fe XXIII to 2.6 au in Fe XVII. The contributions to the cross sections from long-range potentials in the outer region solutions have been accounted for in all ions.

4.1. Photoabsorption and photoionization

The photoabsorption cross sections of Fe XVII and Fe XXIII computed with and without damping are shown in Fig. 1. They are similar to those given in Papers I and III. It may be seen that the cross sections near the K threshold are dominated by a series of symmetric resonances of constant width that cause the smearing of the edge. This unusual resonance behavior, as explained in Paper III, is a consequence of the dominance of Kα and KLL dampings which are practically independent

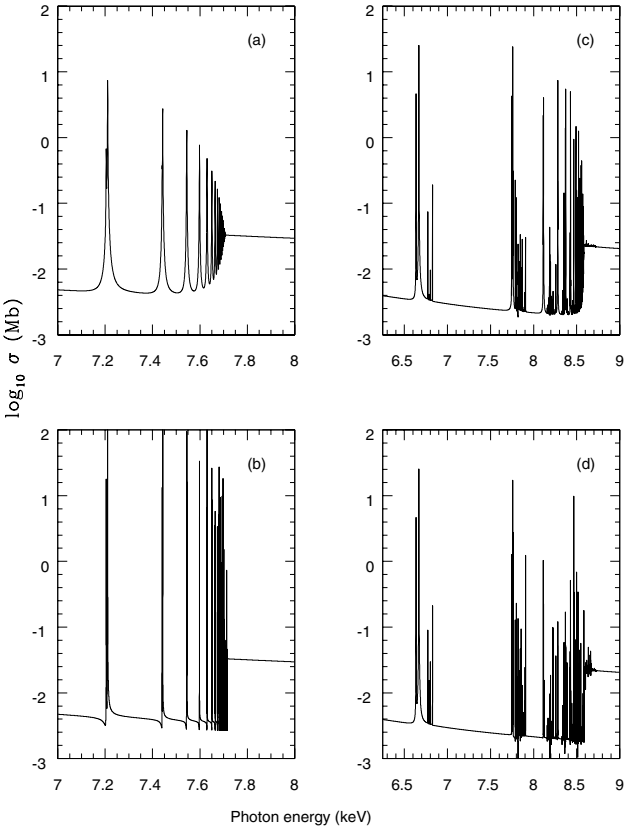

Fig. 1. High-energy total photoabsorption cross sections of the ground level of: **a)** Fe XVII including radiative and Auger damping effects; **b)** Fe XVII excluding damping effects for resonances with $n > 2$; **c)** Fe XXIII including damping; **d)** Fe XXIII excluding damping for resonances with $n > 2$. It may be appreciated that when damping is included the resonance widths are constant for high n leading to a smearing of the K edge.

of the resonance principal quantum number. The present target models are represented with configuration levels within the $n = 2$ complex that can only produce accurate ab initio widths for the Kα resonances. For resonances with $n > 2$, they must be accounted for indirectly with the adjusted optical potential described in Sect. 3.

Total photoabsorption cross sections of the ground states of Fe XVII through Fe XXIII are displayed in Figs. 2, 3. Regular absorption features in ions with electron occupancy $N < 10$ are the Kα resonances. They are absent, however, in Fe XVII due to the full L shell; therefore, the Fe Kα arrays are absorption spectral signatures of highly ionized species. Their energy positions shift with ionic charge from 6.43 keV for Fe XVIII up to 6.63 keV for Fe XXIII. Accurate and complete positions are given in Paper II.

The Kβ $\equiv$ K3 resonances are also distinctive absorption features in the cross sections of Fe ions with 3p subshell vacancies, i.e. for species with $N < 18$. Unresolved transition arrays have been recently observed at ~7.2 keV just below a smeared K edge in the MCG-6-30-15 spectrum (Pounds & Reeves 2002) that can be assigned an Fe Kβ identification. Moreover, the fitted ionization parameter value in

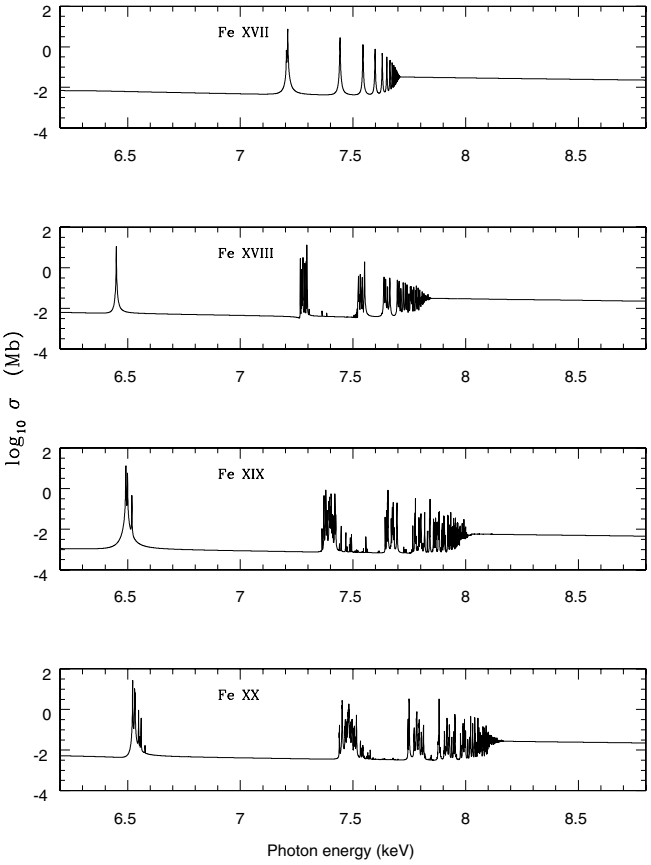

Fig. 2. High-energy total photoabsorption cross section of the ground levels of Fe XVII, Fe XVIII, Fe XIX and Fe XX.

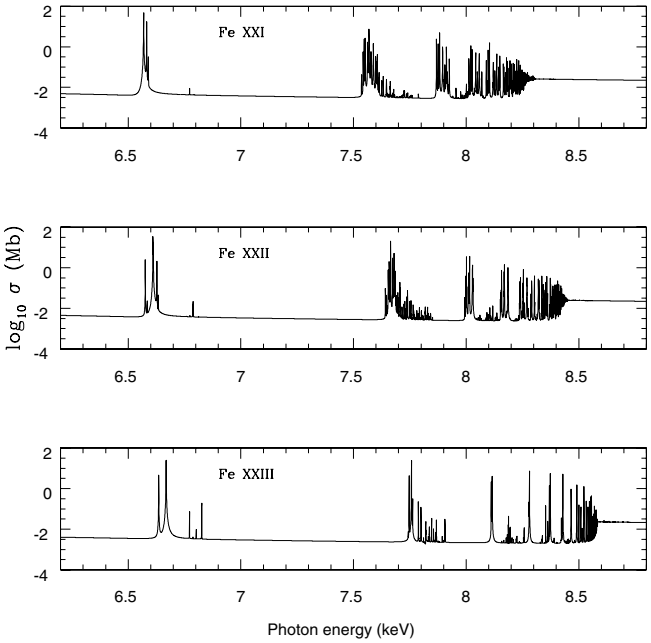

Fig. 3. High-energy total photoabsorption cross section of the ground levels of Fe XXI, Fe XXII and Fe XXIII.

Pounds & Reeves (2002) of $\xi \sim 5.9$ obtained for a warm absorber supports this identification.

As explained in Paper I, when radiation damping is taken into account photoabsorption and photoionization processes must be treated separately. In the former, the integrated cross section under the resonance must remain constant in spite of the broadening caused by damping so as to conserve oscillator strength. In the latter, the cross section is actually reduced since radiation damping leads to radiative de-excitation instead of photoionization. Unfortunately, there is as yet no formal procedure to separate the radiative de-excitation component in BPRM. We use AUTOSTRUCTURE to compute total photoionization cross sections by estimating a central-field background cross sections, representing resonances assuming Lorentzian profiles and computing resonance positions, radiative decay rates and Auger widths in the isolated resonance approximation. We have already shown in Paper I that the photoabsorption cross sections computed with this method closely resembles the cross sections obtained with BPRM.

Partial photoionization cross sections of the fine-structure levels of the ground multiplets leaving the remnant ion in a K-vacancy level have been computed for Fe XVII through Fe XXIII. As an example, in Fig. 4 we plot the photoionization cross sections for transitions from the $[2p]^3\ ^4S^o_{3/2}$ ground level of Fe XX to the first twelve K-vacancy levels of Fe XXI (levels 21 through 32 according Table 1 of Paper II). Similar cross sections have been presented in Paper I for transitions from the ground level of Fe XXIII to the K-vacancy levels of Fe XXIV. Inspection leads to the finding that cross sections for transitions to levels with angular momentum j within a given LS multiplet do not split according to the $(2j + 1)$ statistical weights as previously noted by Rau (1976). Also the dominant channels for K-shell photoionization are those that comply with selection rules between the initial and final levels of the remnant ion:

$$\Delta L = 0 \qquad \Delta S = \pm 1/2 \qquad \Delta J = \pm 1/2, \pm 3/2. \qquad (13)$$

Therefore, in the photoionization of the $[2p]^3\ ^4S^o_{3/2}$ ground level of Fe XX, the dominant channels are those leaving Fe XXI in the $[1s][2p]^3\ ^5S^o_2$ and $[1s][2p]^3\ ^3S^o_1$ K-vacancy levels.

4.2. Electron impact inner-shell excitation

Collision strengths and Maxwellian averaged effective collision strengths have been calculated for excitations to K-vacancy levels in Fe XVIII–Fe XXIII. Collision strengths for Fe XXIV were already reported in Paper I. Collision strengths have been computed up to energies ~2000 Ryd. At such high energies special care must be taken to guarantee adequate convergence of the partial waves expansions. Following the approach in Paper I, we compute partial waves up to $J = 21/2$ or 22/2 followed by non-exchange calculations for higher partial waves up to $J \sim 59/2$ or 60/2. Topping up of partial waves up to infinity for dipole allowed transitions is carried out with the Coulomb-Bethe procedure of Burgess (1974).

In Fig. 5 collision strengths computed with and without damping (radiative and Auger) are presented for the three strongest transitions from the ground level of Fe XIX, i.e. $[2p]^2\ ^3P_2 \rightarrow [1s][2p]\ ^3P^o_j$. It may be appreciated that when damping is taken into account resonances are practically

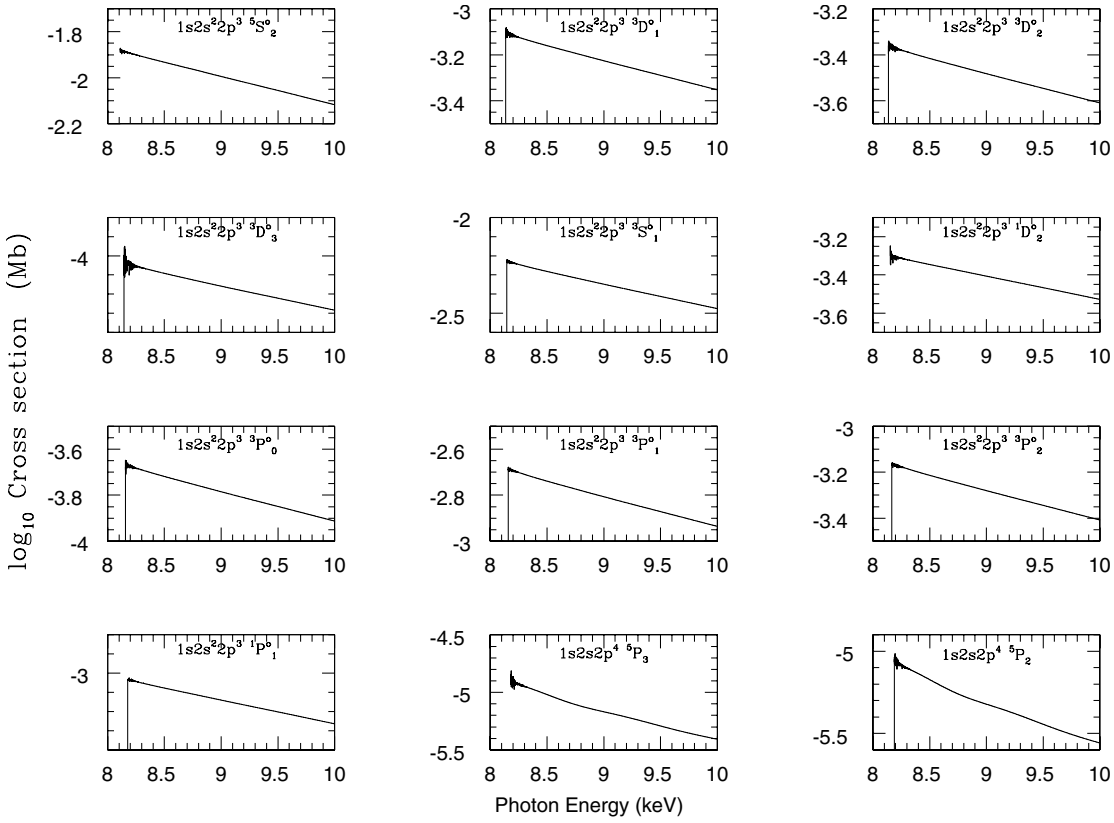

Fig. 4. Partial photoionization cross sections from the $[2p]^3\ ^4S^o_{3/2}$ ground level of Fe XX to the first twelve K-vacancy levels of Fe XXI.

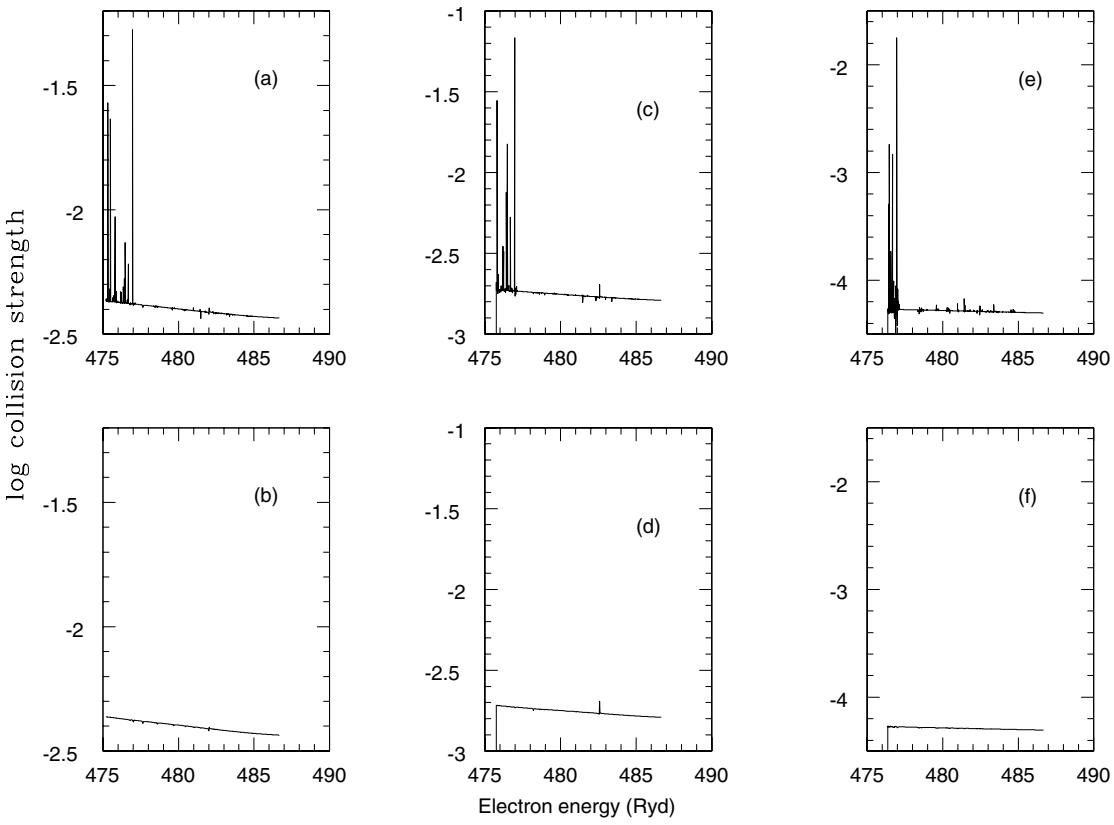

Fig. 5. Comparison of electron impact collision strengths computed with the BPRM method for K-shell excitation of the $[2p]^2\ ^3P_2$ ground level of Fe XIX to the following upper levels: **a)** [1s][2p] $^3P^o_2$ excluding damping; **b)** [1s][2p] $^3P^o_2$ including damping; **c)** [1s][2p] $^3P^o_1$ excluding damping; **d)** [1s][2p] $^3P^o_1$ including damping; **e)** [1s][2p] $^3P^o_0$ excluding damping; and **f)** [1s][2p] $^3P^o_0$ including damping. It may be seen that when damping is taken into account the resonance contribution is essentially washed out.

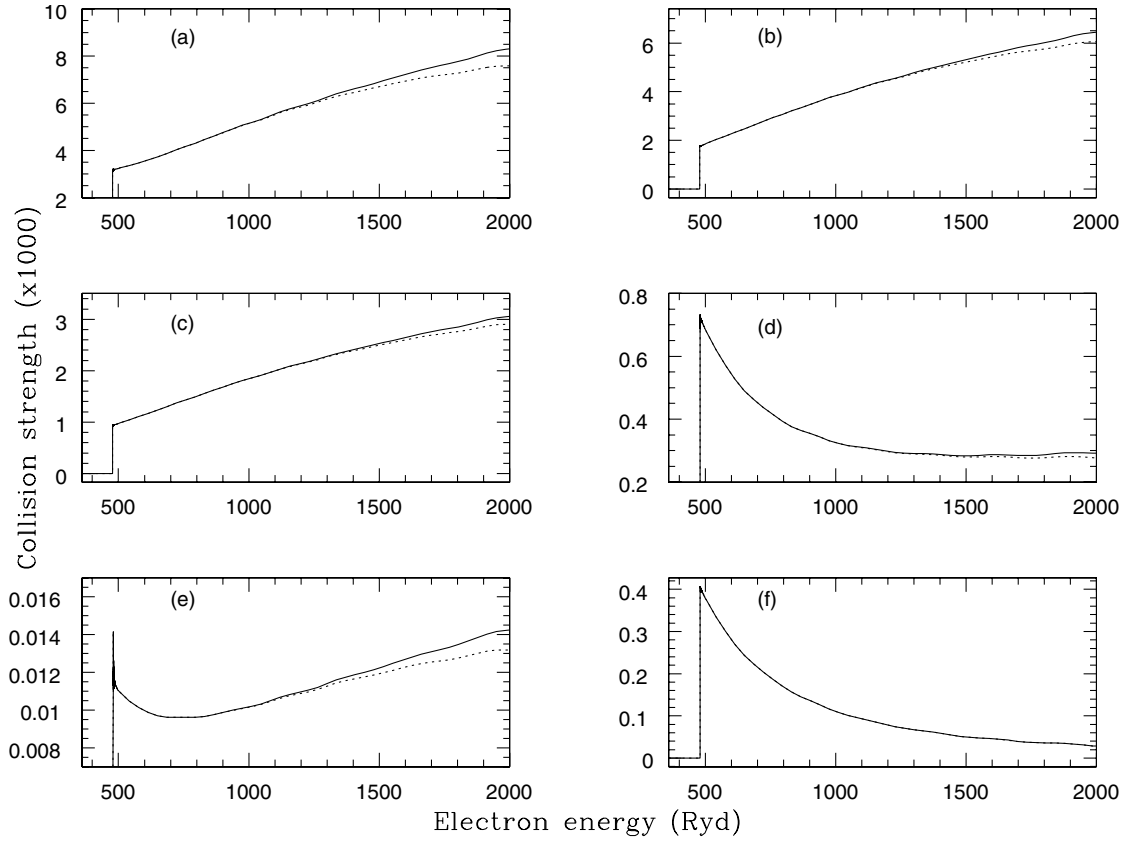

Fig. 6. A selection of collision strengths for Fe XX that shows the contributions of high partial waves at high energies. Dotted lines depict collision strengths obtained with $J \leq 22/2$ while the solid lines those that have been fully topped up to $J = \infty$. **a)** $[2p]^3\ ^4S^o_{3/2}$–$[1s][2p]^2\ ^4P_{5/2}$; **b)** $[2p]^3\ ^4S^o_{3/2}$–$[1s][2p]^2\ ^4P_{3/2}$; **c)** $[2p]^3\ ^4S^o_{3/2}$–$[1s][2p]^2\ ^4P_{1/2}$; **d)** $[2p]^3\ ^4S^o_{3/2}$–$[1s][2p]^2\ ^2D_{3/2}$; **e)** $[2p]^3\ ^4S^o_{3/2}$–$[1s][2p]^2\ ^2D_{5/2}$; **f)** $[2p]^3\ ^4S^o_{3/2}$–$[1s][2p]^2\ ^2P_{1/2}$.

washed out. This effect, first reported in the electron impact excitation of Fe XXIV in Paper I, is observed in the collision strengths of all ions considered here, and it may be then concluded that resonances are essentially irrelevant in electron impact K-shell excitation of highly ionized Fe ions.

To illustrate the convergence of collision strengths with the partial waves expansion, we compare in Fig. 6 a sample of collision strengths for Fe XX that include contributions up to $J = 22/2$ with those topped up to $J = \infty$. The plots show how the contributions from high partial waves become increasingly important with electron energy. It may be also appreciated that the partial waves expansion converges much more slowly for dipole allowed transitions than for those of the forbidden type.

Excitation rates are given in terms of effective collision strengths which are obtained by averaging the collision strengths over a Maxwellian electron velocity distribution

$$\Upsilon_{if}(T) = \int_0^\infty \Omega_{if} \mathrm{e}^{-\epsilon_f/kT} \mathrm{d}(\epsilon_f/kT) \tag{14}$$

where Ω_{if} is the collision strength for the transition $i \rightarrow f$ and ϵ_f is the energy of the outgoing electron. Effective collision strengths up to the infinite temperature limit are computed for excitations to all the $n = 2$ K transitions. Partial waves convergence is tested by mapping the effective collision strength $\Upsilon(T)$ to the reduced form $\Upsilon_\mathrm{r}(T_\mathrm{r})$ where the infinite temperature T range is scaled to the finite interval $0 \leq T_\mathrm{r} \leq 1$ (Burgess & Tully 1992). For an allowed transition the scaling is given by the relations

$$T_\mathrm{r} = 1 - \frac{\ln(c)}{\ln(\kappa T/\Delta E + c)} \tag{15}$$

$$\Upsilon_\mathrm{r}(T_\mathrm{r}) = \frac{\Upsilon(T)}{\ln(\kappa T/\Delta E + \mathrm{e})} \tag{16}$$

with ΔE being the transition energy, κ the Boltzmann constant and c an adjustable scaling parameter. For an electric dipole transition the important limit points are

$$\Upsilon_\mathrm{r}(0) = \Omega(0) \tag{17}$$

$$\Upsilon_\mathrm{r}(1) = \frac{4gf}{\Delta E} \tag{18}$$

where gf is the weighted oscillator strength for the transition. Similarly, for a forbidden transition the scaling relations are given by

$$T_\mathrm{r} = \frac{\kappa T/\Delta E}{\kappa T/\Delta E + c} \tag{19}$$

$$\Upsilon_\mathrm{r}(T_\mathrm{r}) = \Upsilon(E) \tag{20}$$

with the following limit points:

$$\Upsilon_\mathrm{r}(0) = \Omega(0) \tag{21}$$

$$\Upsilon_\mathrm{r}(1) = \Omega_\mathrm{CB} \tag{22}$$

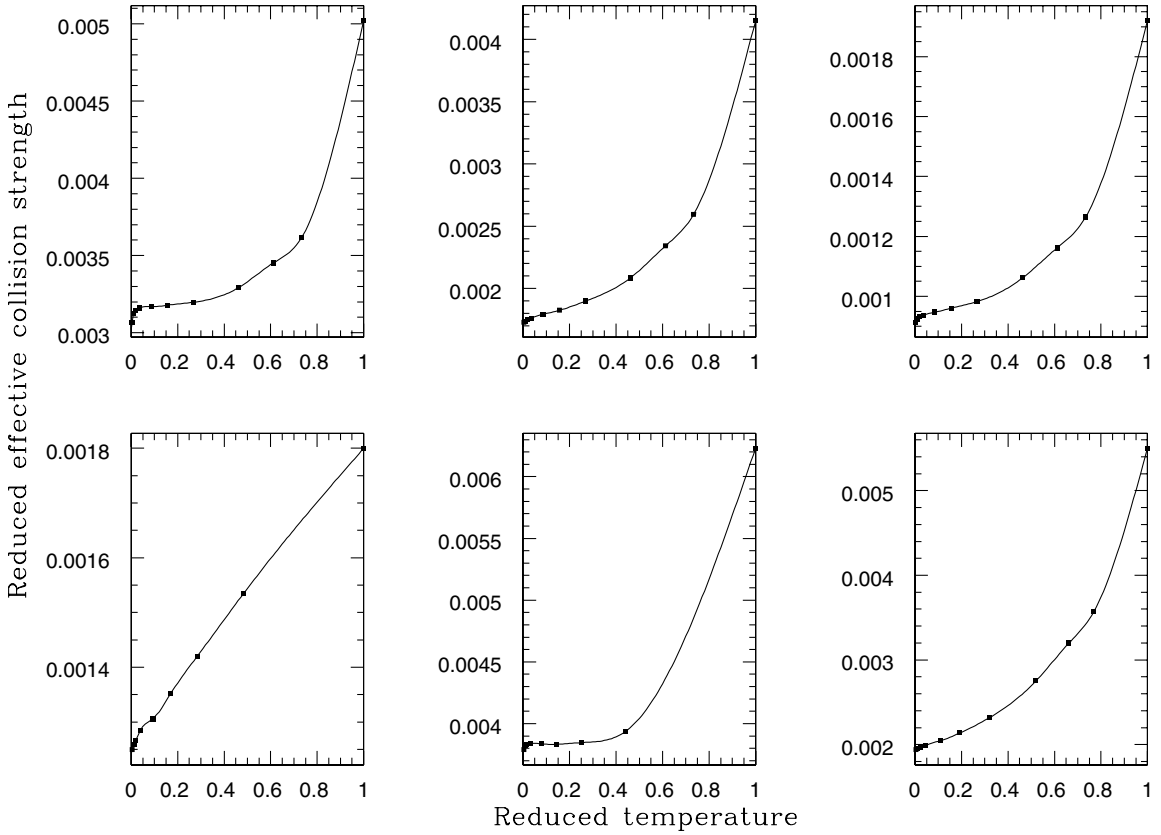

Fig. 7. Samples of electron impact effective collision strengths plotted with the reduced scales of Burgess & Tully (1992). **a)** Fe XX $[2p]^3\ {}^4S^o_{3/2}-[1s][2p]^2\ {}^4P_{5/2}$; **b)** Fe XX $[2p]^3\ {}^4S^o_{3/2}-[1s][2p]^2\ {}^4P_{3/2}$; **c)** Fe XX $[2p]^3\ {}^4S^o_{3/2}-[1s][2p]^2\ {}^4P_{1/2}$; **d)** Fe XXI $[2p]^4\ {}^3P_0-[1s][2p]^3\ {}^3D^o_1$; **e)** Fe XIX $[2p]^2\ {}^3P_2-[1s][2p]\ {}^3P^o_2$; and **f)** Fe XXIII $2s^2\ {}^1S_0-[1s]2p\ {}^1P^o_1$.

where Ω_{CB} is the Coulomb-Born high-energy limit. The gf and Ω_{CB} have been computed with AUTOSTRUCTURE with approximation AST1 of Paper II. In Fig. 7, scaled effective collision strengths for allowed transitions arising from their ground states of Fe XX and Fe XXIII are plotted. The scaling c parameter of Eqs. (15) and (19) has been adjusted so as to characterize the approach to the high temperature limit and to verify convergence. It may be noted that there are no previous data available for comparison. Complete data sets of effective collision strengths, high-temperature limits and A-values for Fe XVIII–Fe XIII are listed in the electronic Tables 1–6.

5. Summary and conclusions

As a part of a project to compute accurate atomic data for the spectral modeling of Fe K lines, electron impact collision strengths and total and partial photoionization cross sections have been computed for K-shell excitation in Fe XVII–Fe XXIII. Radiative and spectator Auger dampings are taken into account in detail which, confirming the findings in Paper III, cause the resonances converging to the K edge of the photoabsorption cross to display a peculiar behavior that leads to edge smearing. This edge behavior appears to have diagnostic potential in astrophysical plasmas. In agreement with previous conclusions by Rau (1976), we find that geometrical angular momentum factors combined with relativistic effect cause the level splitting of the LS photoionization cross sections to depart from statistical weight ratios. Also the prescribed selection rules for the dominant channels for K-shell photoionization are verified. These rules will help to simplify the computations for the lowly ionized members of the Fe isonuclear sequence that would otherwise prove computationally intractable.

With regards to electron impact excitation, resonances are shown to be practically washed out by the effects of radiative and Auger dampings, and thus contribute negligibly to the collisional excitation to $n = 2$ K states. Instead, radiative decay of K states leaving the outer most electrons as spectators results in excitations of either highly excited bound states or high-n 2s vacancy states that tend to autoionize. Furthermore, spectator Auger decay of resonances enhances collisional ionization at the expense of excitation.

The data sets provided here together with the energy levels and radiative and Auger rates reported in Paper II will help modelers to carry out detailed studies of iron K emission for the Fe ions reported so far. Similar calculations for the lower ionization stages are in progress. All the data reported here are being made available directly from TIPTOPbase[1] and from the XSTAR atomic database (Bautista & Kallman 2001).

Acknowledgements. Support for this research was provided in part by grants from the NASA Astrophysics Theory Program and from FONACIT, Venezuela, under contract No. S1-20011000912.

[1] `http://heasarc.gsfc.nasa.gov/topbase`

References

Badnell, N. R. 1986, J. Phys. B, 19, 3827
Badnell, N. R. 1997, J. Phys. B, 30, 1
Ballance, C. P., Badnell, N. R., & Berrington, K. A. 2001, J. Phys. B, 34, 3287
Bautista, M. A., & Kallman, T. R. 2001, ApJS, 134, 139
Bautista, M. A., Mendoza, C., Kallman, T. R., & Palmeri, P. 2003, A&A, 403, 339
Berrington, K. A., & Ballance, C. 2001, J. Phys. B, 34, 2697
Berrington, K. A., Burke, P. G., Butler, K., et al. 1987, J. Phys. B, 20, 6379
Berrington, K. A., Burke, P. G., Chang, J. J., et al. 1974, Comput. Phys. Commun., 8, 149
Berrington, K. A., Burke, P. G., Le Dourneuf, M., et al. 1978, Comput. Phys. Commun., 14, 367
Berrington, K. A., Eissner, W. B., & Norrington, P. H. 1995, Comput. Phys. Commun., 92, 290
Berrington, K., Quigley, L., & Zhang, H. L. 1997, J. Phys. B, 30, 5409
Burgess, A. 1974, J. Phys. B, 7, L364
Burgess, A., & Tully, J. A. 1992, A&A, 254, 436
Burke, P. G., Hibbert, A., & Robb, W. D. 1971, J. Phys. B, 4, 153
Burke, P. G., & Seaton, M. J. 1971, Meth. Comp. Phys., 10, 1
Donnelly, D. W., Bell, K. L., Scott, M. P., et al. 2000, ApJ, 531, 1168
Eissner, W., Jones, M., & Nussbaumer, H. 1974, Comput. Phys. Commun., 8, 270
Eissner, W., & Nussbaumer, H. 1969, J. Phys. B, 2, 1028
Gorczyca, T. W. 2000, Phys. Rev. A, 61, 024702
Gorczyca, T. W., & Badnell, N. R. 1996, J. Phys. B, 29, L283
Gorczyca, T. W., & Badnell, N. R. 2000, J. Phys. B, 33, 2511
Gorczyca, T. W., & McLaughlin, B. M. 2000, J. Phys. B, 33, L859
Mendoza, C., Kallman, T. R., Bautista, M. A., & Palmeri, P. 2004, A&A, 414, 377
Palmeri, P., Mendoza, C., Kallman, T. R., & Bautista, M. A. 2002, ApJ, 577, L119
Palmeri, P., Mendoza, C., Kallman, T. R., & Bautista, M. A. 2003a, A&A, 403, 1175
Palmeri, P., Mendoza, C., Kallman, T. R., et al. 2003b, A&A, 410, 359
Pounds, K. A., & Reeves, J. N. 2002 [arXiv:astro-ph/0201436]
Rau, A. R. P. 1976, in Electron and photon interactions with atoms, ed. H. Kleinpoppen, & M. R. C. McDowell (New York: Premium), 141
Robicheaux, F., Gorczyca, T. W., Pindzola, M. S., et al. 1995, Phys. Rev. A, 52, 1319
Scott, N. S., & Burke, P. G. 1980, J. Phys. B, 13, 4299
Scott, N. S., & Taylor, K. T. 1982, Comput. Phys. Commun., 25, 347